

# Diamond, former coesite and supersilicic garnet in metasedimentary rocks from the Greek Rhodope: a new ultrahigh-pressure metamorphic province established

Evripidis D. Mposkos<sup>a</sup>, Dimitris K. Kostopoulos<sup>b,\*</sup>

<sup>a</sup> Department of Mining and Metallurgical Engineering, Section of Geological Sciences, National Technical University, 9 Heron Polytechniou, Zografou, Athens GR-15780, Greece

<sup>b</sup> School of Geology, Department of Mineralogy, Petrology and Economic Geology, Aristotle University of Thessaloniki, Thessaloniki GR-54006, Greece

Received 15 April 2001; received in revised form 19 June 2001; accepted 10 August 2001

## Abstract

We report here the first discovery of ultrahigh-pressure (UHP) indicator minerals and textures from the Rhodope Metamorphic Province (RMP), northern Greece. In particular, we document the exsolution of quartz, rutile and apatite in sodic garnet from metapelites (garnet–biotite–kyanite gneisses), which attests to the presence of a Si–Ti–Na–P-rich precursor garnet phase. Similar textures in garnet have been reported in the literature only once before for eclogites from the Su Lu UHP metamorphic province, China. We also document the presence of microdiamonds and multicrystalline quartz pseudomorphs after coesite, included in garnet from both eclogites and metapelites. We then argue that these rocks had once been transported to depths exceeding 220 km, well into the upper mantle, thus establishing the RMP as another important UHP metamorphic belt in the world. © 2001 Elsevier Science B.V. All rights reserved.

**Keywords:** ultrametamorphism; diamond; garnet; majorite; coesite; Rhodope Greece; Greece

## 1. Introduction

The hypothesis of ultrahigh-pressure (UHP) metamorphism of crustal rocks was first put forward to explain the formation of mantle-equilibrated (4.5 GPa/850°C) olivine-free, orthopyrox-

ene eclogites of gabbroic composition from Norway [1]. However, up until the discovery of coesite in crustal lithologies [2,3] the subduction of continental material to depths below the crust–mantle boundary was considered impossible. The presence of coesite hinted at the possibility that continental material can be transported to depths of at least 85–95 km (i.e. 2.6–3.0 GPa at 600–1100°C [4]). The documentation of diamond in crustal metamorphic rocks from several continental plate collision zones [5–10] indicated continental subduction to even greater mantle depths (i.e. 100–150 km or 3.1–4.5 GPa at 600–1100°C [11]). Ad-

\* Corresponding author. Tel.: +30-31-099-81-42;  
Fax: +30-31-099-84-74.

E-mail addresses: mposkos@metal.ntua.gr (E.D. Mposkos),  
mimis@geo.auth.gr (D.K. Kostopoulos).

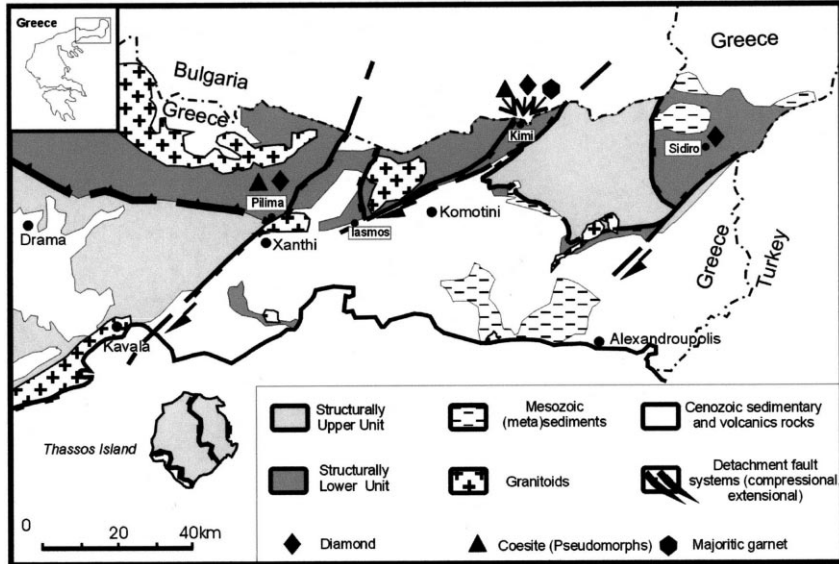


Fig. 1. Geological map of the central and eastern Greek Rhodope (after [23]; simplified) with locations of samples containing diamond, former coesite, and supersilicic garnet.

ditional evidence for ultrahigh metamorphic pressures came from detailed microstructural observations, particularly from the identification of:

1.  $\alpha\text{-PbO}_2$ -type  $\text{TiO}_2$  inclusions in garnet from diamondiferous gneisses [12], requiring pressures in the range 4.5–6.5 GPa at 1000°C [13];
2. clinopyroxene, rutile and apatite exsolutions in garnet from eclogites, suggesting the existence of precursor majorite stable at depths exceeding 200 km [14];
3. ilmenite exsolutions in olivine and clinoenstatite exsolutions in diopside from Alpine-type garnet lherzolites, implying minimum depths of origin of 250 km [15,16];
4. two-pyroxene and rutile exsolutions in garnet from Alpine-type garnet lherzolites pointing to an initial majorite composition stable at  $P > 6$  GPa [17,18];
5. oriented magnetite lamellae in olivine from Alpine-type harzburgites, indicating exsolution from a pre-existing wadsleyite phase stable at  $P > 6$  GPa [19].

Here, we report the first discovery of diamond and former coesite inclusions in garnet, and of quartz, rutile and apatite exsolutions in sodic gar-

net from eclogites and metapelites of the Rhodope Metamorphic Province (RMP), northern Greece. We then argue that these rocks attained peak metamorphic  $P$ - $T$  conditions of about 7 GPa/1100°C.

## 2. Geological background

The RMP is one of the major geotectonic units of northern Greece (Fig. 1). It extends northwards into eastern former Yugoslavia and southern Bulgaria, and includes the Serbo-Macedonian (western RMP) and Rhodope Massifs (central and eastern RMP). It mainly comprises amphibolites, often enclosing eclogite bodies, amphibolite-facies para- and orthogneisses and schists, in places migmatitic, and marbles, all invariably intruded by large granitic masses. The RMP has traditionally been viewed as a stable continental block, consolidated in Precambrian to Paleozoic times. Recent structural and petrologic work has nevertheless shown the RMP in fact to be a complex of Alpine synmetamorphic nappes characterized by south to southwestward stacking and associated with both coeval and subsequent extension in an Alpine active margin setting [20–22].

On the basis of calculated metamorphic  $P-T$  paths and exhumation age criteria for the various metamorphic rocks the RMP has been subdivided into distinct entities [23]. However, for the purpose of the present paper, and to avoid unnecessary complexity, these entities have been grouped into two units, a structurally upper and a structurally lower unit (see Fig. 1). In terms of exhumation ages the structurally upper unit appears to have been exhumed earlier (65–30 Ma) compared to the structurally lower unit (30–8 Ma), which also constitutes the so-called ‘Rhodope metamor-

phic core complex’. In terms of metamorphic  $P-T$  paths the major difference between the structurally lower and the structurally upper unit is that in the latter, prograde assemblages developed at  $T > 550^\circ\text{C}$ , whereas in the former they developed at  $T < 550^\circ\text{C}$ . Available peak pressure estimates range from ca. 1.2–1.4 GPa for the structurally lower unit to about 1.6–1.9 GPa for the structurally upper unit [23]. However, the recent discovery of graphitized diamonds in metamorphosed crustal rocks (of both sedimentary and igneous protoliths) forming the westernmost extension of

Table 1

EMP analyses (wt%) of selected mineral inclusions and host garnet (ordinary and supersilicic) from grt–bt–ky gneisses, Kimi area (samples OS-3 and OS-4), and of supersilicic garnet produced experimentally at 7 GPa/1100°C on a pelitic composition ([38]; run # sh23)

|                                | Ky<br>incl. in<br>grt | Ap<br>incl. in<br>grt | Rt<br>incl. in<br>grt brown | Rt<br>incl. in<br>grt blue | Bt<br>incl. in<br>grt | Grt<br>ordinary | Grt<br>supersilicic<br>Rhodope | Grt<br>supersilicic<br>experimental |
|--------------------------------|-----------------------|-----------------------|-----------------------------|----------------------------|-----------------------|-----------------|--------------------------------|-------------------------------------|
| SiO <sub>2</sub>               | 36.48                 |                       |                             | 0.43                       | 37.25                 | 37.47           | 38.52                          | 39.89                               |
| TiO <sub>2</sub>               |                       |                       | 94.81                       | 95.96                      | 2.62                  |                 | 1.03                           | 1.02                                |
| Al <sub>2</sub> O <sub>3</sub> | 61.10                 |                       |                             |                            | 18.12                 | 21.45           | 19.58                          | 20.38                               |
| Fe <sub>2</sub> O <sub>3</sub> | 0.70                  |                       |                             |                            |                       |                 |                                |                                     |
| FeO                            |                       | 0.25                  | 1.26                        | 1.44                       | 12.86                 | 29.72           | 31.65                          | 24.92                               |
| MnO                            |                       |                       |                             |                            |                       | 0.92            | 2.06                           |                                     |
| MgO                            | 0.34                  | 0.83                  | 0.35                        |                            | 15.24                 | 5.84            | 3.87                           | 5.04                                |
| CaO                            |                       |                       | 52.25                       |                            |                       | 3.80            | 2.80                           | 8.47                                |
| Na <sub>2</sub> O              |                       |                       |                             |                            | 0.46                  |                 | 0.60                           | 0.62                                |
| K <sub>2</sub> O               |                       |                       |                             |                            | 8.74                  |                 |                                | 0.11                                |
| P <sub>2</sub> O <sub>5</sub>  |                       | 44.06                 |                             |                            |                       |                 | 0.33                           |                                     |
| V <sub>2</sub> O <sub>5</sub>  |                       |                       | 2.16                        | 1.47                       |                       |                 |                                |                                     |
| Total                          | 98.55                 | 97.38                 | 98.58                       | 99.30                      | 95.28                 | 99.20           | 100.44                         | 100.45                              |
| Si                             | 1.0007                |                       |                             | 0.0058                     | 2.7322                | 2.9724          | 3.0530                         | 3.0795                              |
| Ti                             |                       |                       | 0.9652                      | 0.9698                     | 0.1445                |                 | 0.0614                         | 0.0592                              |
| Al                             | 1.9754                |                       |                             |                            | 1.5666                | 2.0054          | 1.8290                         | 1.8543                              |
| Fe <sup>3+</sup>               | 0.0144                |                       |                             |                            |                       |                 |                                |                                     |
| Fe <sup>2+</sup>               |                       | 0.0184                | 0.0143                      | 0.0162                     | 0.7886                | 1.9716          | 2.0978                         | 1.6088                              |
| Mn                             |                       |                       |                             |                            |                       | 0.0618          | 0.1383                         |                                     |
| Mg                             | 0.0139                | 0.1080                | 0.0071                      |                            | 1.6666                | 0.6906          | 0.4573                         | 0.5800                              |
| Ca                             |                       | 4.9176                |                             |                            |                       | 0.3230          | 0.2378                         | 0.7006                              |
| Na                             |                       |                       |                             |                            | 0.0647                |                 | 0.0922                         | 0.0928                              |
| K                              |                       |                       |                             |                            | 0.8179                |                 |                                | 0.0108                              |
| P                              |                       | 2.9824                |                             |                            |                       |                 | 0.0202                         |                                     |
| V                              |                       |                       | 0.0193                      | 0.0131                     |                       |                 |                                |                                     |
| Total                          | 3.0044                | 8.0264                | 1.0058                      | 1.0048                     | 7.7813                | 8.0249          | 7.9870                         | 7.9860                              |
| $X_{\text{Grs}}$               |                       |                       |                             |                            |                       | 0.1060          | 0.0811                         | 0.2425                              |
| $X_{\text{Alm}}$               |                       |                       |                             |                            |                       | 0.6471          | 0.7157                         | 0.5568                              |
| $X_{\text{Prp}}$               |                       |                       |                             |                            |                       | 0.2267          | 0.1560                         | 0.2007                              |
| $X_{\text{Sp}}$                |                       |                       |                             |                            |                       | 0.0203          | 0.0472                         |                                     |

Atoms per formula unit for individual minerals were calculated on the basis of the following numbers of oxygens: ky (five O); ap (12.5 O); rt (two O); bt (11 O); grt (12 O).

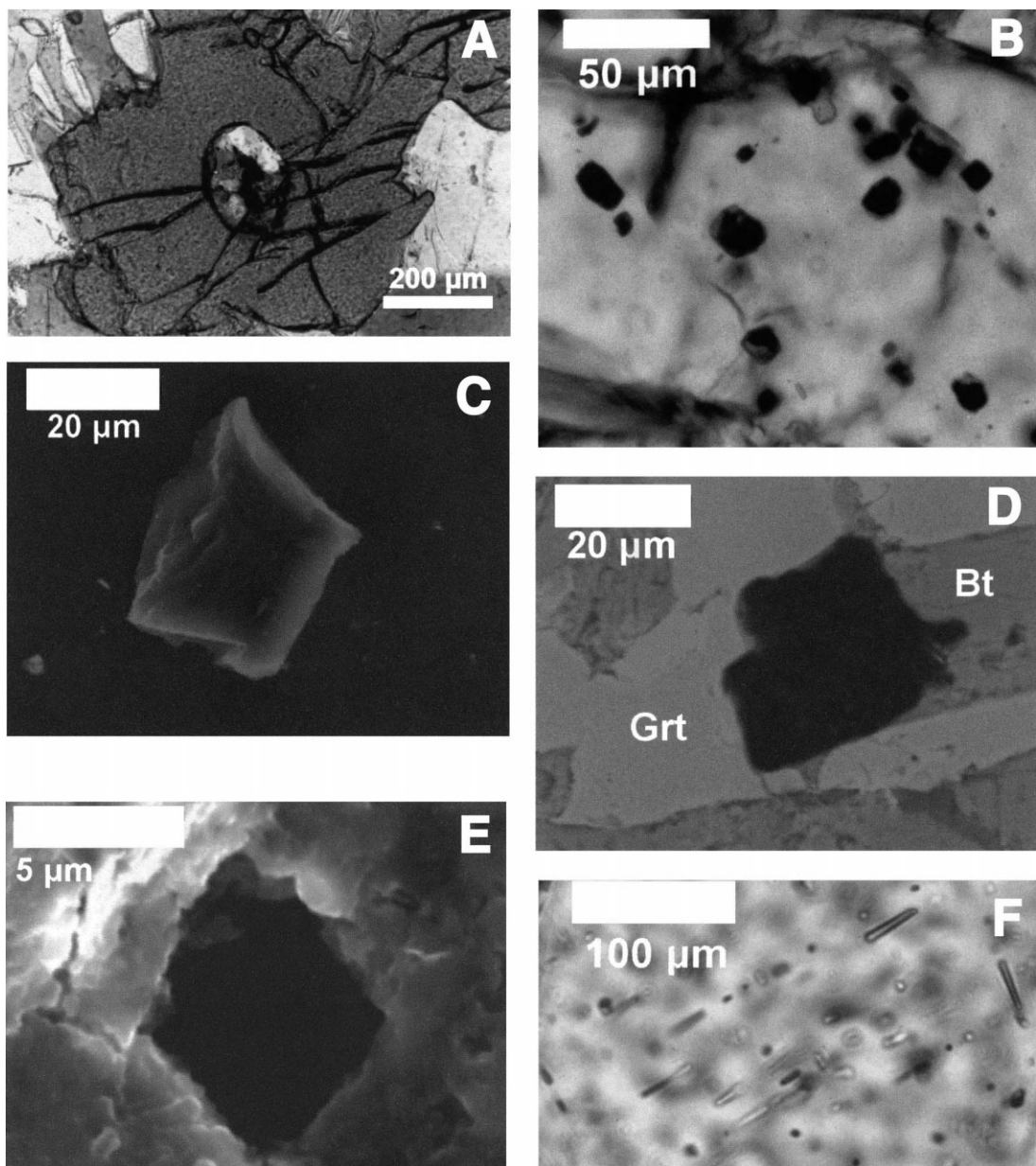


Fig. 2.

Rhodope thrust units near Thessaloniki [24] signified that the individual  $P$ - $T$  paths published hitherto for the various entities of the structurally upper unit should, instead, be regarded only as the final part of their respective exhumation histories.

### 3. Petrography of UHP sedimentary lithologies

UHP sedimentary lithologies were discovered in the structurally upper unit of the RMP as exemplified above, and particularly at its central and eastern parts (see Fig. 1). They comprise garnet-

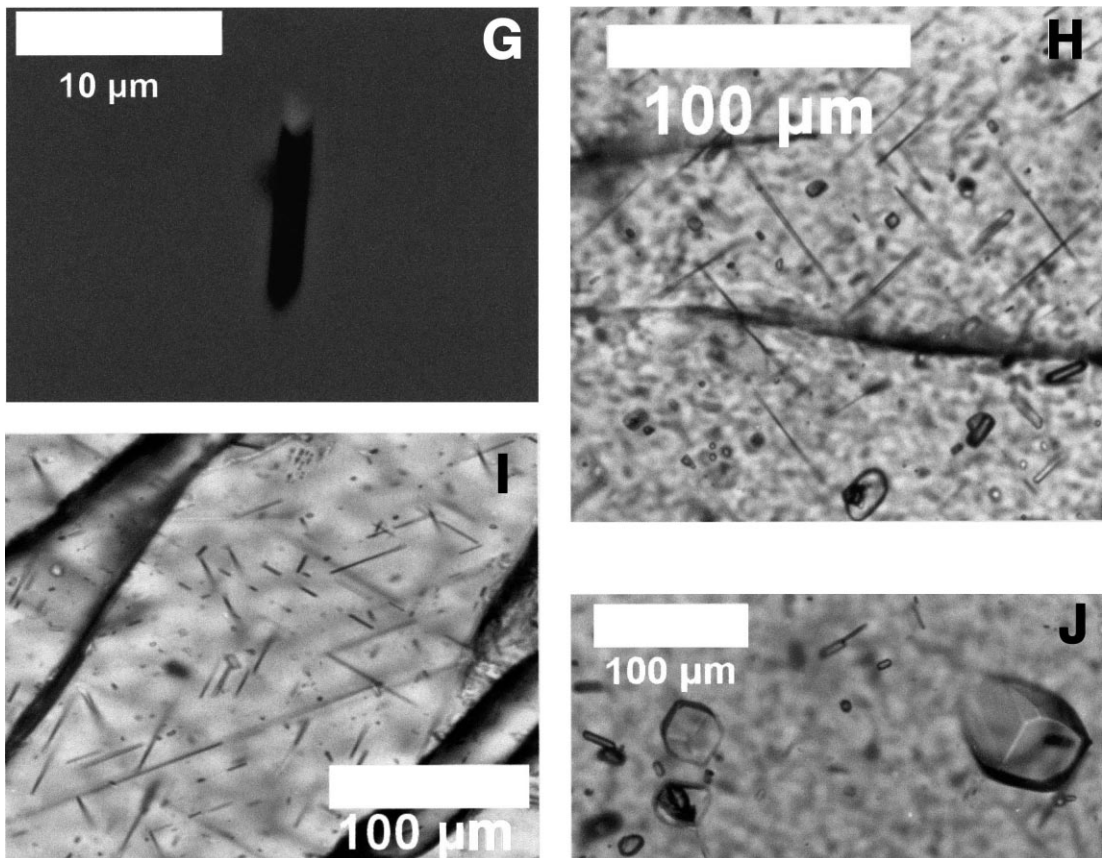


Fig. 2. (A) Photomicrograph of MPQ, pseudomorphic after coesite, included in garnet. Note the radial fracturing of the garnet host. Amphibolitized eclogite (sample OS-4C); Kimi area. (B) Photomicrograph of microdiamond inclusions in garnet porphyroblast. Some of the diamonds show well-developed octahedral crystal faces. Grt–bt–ky gneiss (sample XTH-1); Pilima area. (C) SE image of octahedral diamond included in potassic white mica. Grt–bt–ky gneiss (sample XTH-1); Pilima area. (D) BSE image of two superposed octahedral diamonds included in garnet and biotite. Grt–bt–ky gneiss (sample XTH-1); Pilima area. (E) SE image of octahedral diamond included in garnet porphyroblast. Grt–ky–st–chl schist (sample PS-11C); Sidiro area. (F) Photomicrograph of quartz rods exsolved from majoritic garnet (orthogonal pattern). Grt–bt–ky gneiss (sample OS-4A); Kimi area. (G) BSE image of quartz rod exsolved from majoritic garnet. The white spot at the end of the rod is the trace of projection of a rutile needle oriented orthogonal to the quartz rod. Grt–bt–ky gneiss (sample OS-3); Kimi area. (H) Photomicrograph of rutile needles exsolved from majoritic garnet (orthogonal pattern). Grt–bt–ky gneiss (sample OS-3); Kimi area. (I) Photomicrograph of rutile needles exsolved from majoritic garnet (triangular pattern). The needles are oriented parallel to the octahedral faces of the host garnet. Grt–bt–ky gneiss (sample OS-4A); Kimi area. (J) Photomicrograph of apatite exsolved from majoritic garnet. Note the hexagonal prismatic basal sections. Grt–bt–ky gneiss (sample OS-3); Kimi area.

biotite–kyanite gneisses and garnet–kyanite–staurolite–chlorite schists. Selected mineral analyses from the gneisses are listed in Table 1, and a brief account of the petrography of these rocks is given below.

The garnet–biotite–kyanite gneisses are composed of garnet and kyanite porphyroblasts set in a matrix of biotite, muscovite, plagioclase and

quartz. Garnet porphyroblasts are rich in almandine component and measure, on average, 2–5 mm in diameter. They show exsolutions of quartz, rutile and apatite, and carry inclusions of biotite, kyanite, rutile, apatite, quartz, zircon and micro-diamond (see Section 4 for description of exsolutions and microdiamond). Rutile inclusions in garnet are of two kinds, needle-like with a bluish

hue and ordinary brownish prismatic sections. The needle-like blue rutile inclusions contain a small but significant amount of  $\text{SiO}_2$ , the importance of which will be discussed in Section 5. By contrast, the brown rutile inclusions are devoid of silica. Apatite inclusions in garnet are hydroxyapatites containing a small percentage of  $\text{MgO}$  and still less  $\text{FeO}$ . Kyanite inclusions in garnet also contain small amounts of  $\text{Fe}_2\text{O}_3$  and a little  $\text{MgO}$ . Biotite inclusions in garnet display  $\text{Mg}/(\text{Mg}+\text{Fe})$  ratios comparable to those of biotite inclusions in garnet from Kokchetav gneisses [5,25], but are distinctly richer in  $\text{TiO}_2$  and coexist with garnet of much lower  $\text{Mg}/(\text{Mg}+\text{Fe})$  ratios in relation to their Kokchetav counterparts. Aggregates of  $\text{bt} \pm \text{ms} + \text{pl} + \text{ky} + \text{qtz}$  enclosed by garnet and displaying a corroded contact against their host appear to have been formed by replacement of pre-existing phengite inclusions plus garnet wall-rock upon decompression, according to the reaction:  $\text{grt} + \text{phe} = \text{bt} + \text{pl} + \text{ky} + \text{qtz}$ . Garnet porphyroblasts also show resorbed edges, being replaced either by  $\text{bt} + \text{ky}$  or  $\text{bt} + \text{pl}$ . Kyanite porphyroblasts in the gneisses are, on average, 0.5–1 mm long. They are often deformed and contain inclusions of biotite, rutile, quartz, and rarely garnet. Matrix muscovite forms large flakes (1–2 mm long) characterized by exsolution of numerous, oriented rutile needles (sagenite), suggesting a high-Ti, high- $T$  (HT) white mica precursor (Massonne, electronic communication to D.K.K., July 2001). Importantly, a phengite inclusion in garnet from a diamondiferous garnet–zoisite gneiss containing 2.52 wt%  $\text{TiO}_2$  and associated with peak or post-peak high-pressure (HP)/HT conditions has been reported from Kokchetav [25]. Small pockets in the matrix composed of equigranular plagioclase and quartz aggregates, unoriented muscovite and biotite flakes and small kyanite prisms are interpreted to have crystallized directly from a melt phase.

The garnet–kyanite–staurolite–chlorite schists consist of garnet and kyanite porphyroblasts set in a matrix of garnet, staurolite, chlorite, muscovite and quartz. Garnet porphyroblasts (3–5 mm in diameter) contain inclusions of phlogopite, kyanite, quartz, rutile and microdiamond (see Section 4). Kyanite porphyroblasts may reach up to

1 cm in length and are commonly replaced by muscovite and staurolite. Staurolite either rims resorbed kyanite crystals or grows epitaxially on them. Relics of resorbed kyanite are commonly found included in staurolite. Garnet is also replaced by staurolite and chlorite. Biotite is present only as rare inclusions in garnet and is totally lacking from the rock matrix.

#### 4. UHP indicators

In this section we describe UHP metamorphic indicator minerals discovered in crustal rocks belonging to the structurally upper unit of the RMP (see Fig. 1 for the localities discussed henceforth). These include:

1. multicrystalline polygonal quartz [26,27] (MPQ) aggregates included in garnet (Fig. 2A) from amphibolitized eclogites (Kimi and Pilima areas),
2. minute carbon cubes and octahedra mainly included in garnet porphyroblasts (Fig. 2B–E) from garnet–biotite–kyanite gneisses (Kimi and Pilima areas) and garnet–biotite–staurolite–chlorite schists (Sidiro area),
3. rods (or needles) of silica, rutile, and apatite exsolved inside sodic garnet porphyroblasts (Fig. 2F–I) in garnet–biotite–kyanite gneisses (Kimi area).

We have optically identified and subsequently verified (by electron microprobe (EMP) analyses<sup>1</sup> [pure  $\text{SiO}_2$ ]) MPQ aggregates as inclusions in garnet porphyroblasts in amphibolitized eclogites from the Pilima and Kimi areas. Strong sub-

<sup>1</sup> Microprobe analyses were conducted at the Department of Mineralogy, Petrology and Economic Geology, Aristotle University, Thessaloniki, Greece, using a Jeol JSM-840A scanning microscope equipped with an EDS Oxford ISIS 300 analytical system. Operating conditions were: accelerating potential 20 kV, beam current 45 nA and counting time 80 s, with ZAF correction being provided on-line. Standards used were: orthoclase (Si, K), jadeite (Na), corundum (Al), wollastonite (Ca), periclase (Mg), GaP (P), and Fe, Mn, Ti, V, Cr, and Ni metals.

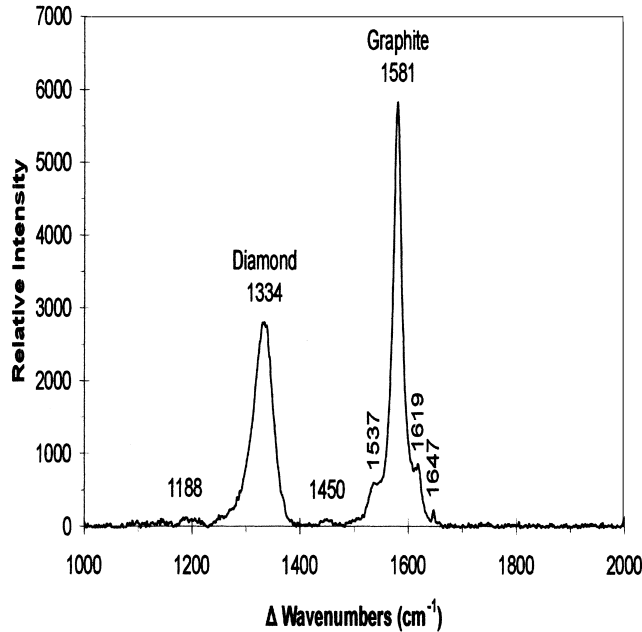


Fig. 3. Laser Raman spectrum of octahedral carbon inclusion in garnet. Grt–bt–ky gneiss (sample XTH-1); Pilima area.

radial cracks emanate from the inclusions (see Fig. 2A). Although MPQ aggregates with radial fractures should be treated with caution, as they are not unique to coesite breakdown [27], the overwhelming evidence for UHP metamorphism in the area (see below) leaves little doubt that they were former single coesite crystals. The preservation of coesite and microdiamond in UHP metamorphic crustal rocks is confined to rigid hosts such as garnet, clinopyroxene or kyanite and depends on various factors, the most important of which are the rate of exhumation, grain size of precursor coesite or diamond, fluid availability [28] and  $P$ - $T$  conditions of superimposed retrograde metamorphism.

As was the case with pseudomorphs after coesite, diamond in RMP rocks was initially identified optically and subsequently verified by both EMP analyses (pure carbon) and in situ laser Raman microspectroscopy. The diamonds appear as minute (average size  $\sim 10 \mu\text{m}$ ) cubo-octahedral inclusions in garnet porphyroblasts from grt–bt–ky gneisses of the Kimi, Sidiro and Pilima areas (Fig. 2B–E). Their mode of occurrence highly resembles that of diamonds in very similar rocks

from the Kokchetav Massif, Kazakhstan [5] (grt–bt  $\pm$  ky  $\pm$  cpx gneisses) and from the Saxonian Erzgebirge, Germany [9] (grt–phe–ky  $\pm$  bt gneisses). Occasionally, the garnets are literally teeming with microdiamonds ( $\sim 30$  per  $1.5 \text{ cm}^2$ ), a feature that has also been observed for the Erzgebirge [9] and Kokchetav [29] garnets.

Fig. 3 shows the Raman spectrum obtained for a carbon octahedron enclosed by porphyroblastic garnet from a grt–bt–ky gneiss of the Pilima area. Two intense bands become immediately apparent, one at  $1334 \text{ cm}^{-1}$  and the other at  $1581 \text{ cm}^{-1}$ , which are diagnostic of diamond [10] and graphite respectively [30,31]. The typical diamond vibration band exhibits an asymmetric distribution with some tailing toward lower frequencies and an important broadening (ca.  $40 \text{ cm}^{-1}$ ) as expected for nanocrystalline domains [32]. By using the variation of the  $F_{2g}$  mode linewidth with particle size [33], the size of the crystallites is estimated at ca.  $47 \text{ \AA}$ . The graphite band (G line) displays a shoulder at  $1619 \text{ cm}^{-1}$ , which is characteristic of disordered, microcrystalline graphite [34,35]. Also visible in the Raman spectrum of Fig. 3 are two weak bands at  $1188$  and  $1450$ ,

and a stronger one at  $1537\text{ cm}^{-1}$ . Similar bands have been observed during transformation of diamond to graphite under non-hydrostatic, contact compressive stress and have been attributed to a certain carbon structure [36]. It should be emphasized that the presence of new Raman bands is the most striking evidence of the phase transformation in diamond [36]. Quantitative evaluation of the amount of graphite carbon formed is complicated due to the fact that the Raman cross-section of graphite is approximately 50 times higher than that of crystalline diamond and hence  $\text{sp}^2$ -bonded regions dominate the Raman spectra even at small amounts of  $\text{sp}^2$  carbon [36].

Perhaps the most important of our discoveries is the identification (by means of optical microscopy, EMP analyses and in situ laser Raman microspectroscopy) of quartz, rutile and apatite exsolution rods (or needles) in porphyroblastic garnet from grt–bt–ky gneisses of the Kimi area. Similar exsolution textures (i.e. clinopyroxene, rutile, and apatite exsolution rods in garnet) have been reported only once in the literature [13] for eclogites – not metapelites – from Yangkou, Su Lu UHP metamorphic province, China. As is the case for the rods in the Yangkou eclogitic garnet, the rods in the Rhodope metapelite garnet also occur in groups of parallel rods along crystallographically controlled planes of the host garnet, thus displaying an orthogonal (Fig. 2F–H) or equilateral triangular pattern in cross-section (Fig. 2I); oriented apatite rods are also observed, as well as hexagonal basal sections (Fig. 2J). The volumes of the exsolved minerals are difficult to assess with accuracy; our estimates are about 4 vol% for quartz, 1 vol% for rutile and 0.9 vol% for apatite. Unfortunately, the very small thickness of the exsolved rutile needles (usually no thicker than  $0.5\text{ }\mu\text{m}$ ) did not allow us to determine its chemical composition with confidence by EMP analysis. The exsolution of quartz, rutile, and apatite is taken here as indicative of the existence of a garnet precursor phase richer than normal in Si, Ti and P, that is, of a ‘majoritic’ garnet [37]. The significance of the presence of diamond, former coesite, and supersilicic garnet in Rhodope crustal metamorphic rocks and the contribution of these phases to evaluating peak

pressures of metamorphism will now be addressed.

## 5. Discussion

In the RMP, the presence of MPQ aggregates as inclusions in porphyroblastic garnet from amphibolitized eclogites is attributed to the breakdown of pre-existing coesite and constrains metamorphic pressures to a minimum of 2.6–2.9 GPa at  $600\text{--}900^\circ\text{C}$  [4]. Moreover, the mere presence of diamonds in porphyroblastic garnet from metapelites dictates metamorphic pressures in excess of 3.1–3.9 GPa at  $600\text{--}900^\circ\text{C}$  [11] for the host rocks. Thus, at a first approximation, minimum depths of 80–140 km for the subduction of the crustal protoliths of the RMP can be inferred by using only mineralogical criteria.

An estimate as to the  $P$ – $T$  conditions that prevailed during formation of pre-existing supersilicic garnet in the RMP grt–bt–ky gneisses may be obtained from experiments on relevant systems and majorite barometry. We have conducted detailed EMP traverses of the rod-bearing garnet porphyroblasts and discovered rare, apparently homogenous domains of ‘majoritic’ composition rich in Si and Ti, as was expected from the nature of the exsolved phases, but, importantly, also in Na (Table 1). Also shown in Table 1 is the composition of garnet produced experimentally at 7 GPa and  $1100^\circ\text{C}$  on a pelite composition [38]. The match is surprisingly good and suggests similar  $P$ – $T$  conditions of formation for the Rhodope ‘majoritic’ garnet. This suggestion is further reinforced by the results obtained ( $7.17 \pm 0.03$  GPa) by applying the recently calibrated Si-in-majorite and (Al+Cr)-in-majorite barometers [37]. Additional support for the proposed extreme pressure conditions under which the almandine-rich Rhodope supersilicic garnet became stabilized is provided by experimental work on pyroxene–garnet solid-solution equilibria in both the pyrope–enstatite and almandine–ferrosilite systems at elevated temperatures and pressures [39]. Reference to Table 1 shows that the Rhodope supersilicic garnet contains ca. 5.3 mol% pyroxene in solid solution, a value which is in excellent agreement with the

experimental solubility of ferrosilite in almandine at 1100°C/7 GPa, having taken into account the slight shift of the garnet solid-solution solvus to higher pressures with increasing temperature (table V and figure 6 in [39]). Worth mentioning here also is the observed silica content of the ‘blue’ needle-like rutile inclusions in the supersilicic Rhodope garnets. SiO<sub>2</sub> in rutile is indicative of HT/HP conditions; it actually represents stishovite component in rutile (Massonne, electronic communication to D.K.K., July 2001). Clearly, further experimental work is needed in this direction to amplify the significance of a potential Si-in-rutile thermobarometer for UHP metamorphic rocks.

Taken collectively, the above pieces of evidence conclusively demonstrate the subduction of the RMP to depths of the order of 220 km and establish the province as one of the most important UHP metamorphic belts in the world.

## Acknowledgements

Prof. I. Chryssoulakis, National Technical University, Athens, Greece, kindly provided access to laser Raman microanalytical facilities. Dr. K. Andrikopoulos helped in obtaining and processing the Raman spectra. Prof. S. Sklavounos and Dr. E. Pavlidou assisted with the EMP analyses and the SEM images. Dr. P. Gautier, Université Rennes 1, France, donated the coesite-bearing amphibolitized eclogite sample from the Pilima area. Constructive journal reviews by Profs. D.C. Smith, Paris, H.W. Green II, CA, USA, and J.E. Dixon, Edinburgh, UK, and fruitful discussions with Prof. H.-J. Massonne, Stuttgart, Germany, are greatly appreciated. Mr. A. Avgirinas is cordially thanked for his CorelDraw expertise in drafting Fig. 1. **[BW]**

## References

- [1] M.A. Lappin, D.C. Smith, Mantle-equilibrated orthopyroxene eclogite pods from the basal gneisses in the Selje district, western Norway, *J. Petrol.* 19 (1978) 530–584.
- [2] C. Chopin, Coesite and pure pyrope in high-grade blueschists of the western Alps: a first record and some consequences, *Contrib. Mineral. Petrol.* 86 (1984) 107–118.
- [3] D.C. Smith, Coesite in clinopyroxene in the Caledonides and its implications for geodynamics, *Nature* 310 (1984) 641–644.
- [4] B.S. Hemingway, S.R. Bohlen, W.B. Hankins, E.F. Westrum Jr., O.L. Kuskov, Heat capacity and thermodynamic properties for coesite and jadeite: reexamination of the quartz-coesite equilibrium boundary, *Am. Mineral.* 83 (1998) 409–418.
- [5] N.V. Sobolev, V.S. Shatsky, Diamond inclusions in garnets from metamorphic rocks: a new environment for diamond formation, *Nature* 343 (1990) 742–746.
- [6] M.L. Leech, W.G. Ernst, Graphite pseudomorphs after diamond? A carbon isotope and spectroscopic study of graphite cuboids from the Maksyutov Complex, south Ural Mountains, Russia, *Geochim. Cosmochim. Acta* 62 (1998) 2143–2154.
- [7] S. Xu, A.I. Okay, S. Ji, A.M.C. Sengör, W. Su, Y. Liu, L. Jiang, Diamond from the Dabie Shan metamorphic rocks and its implication for tectonic setting, *Science* 256 (1992) 80–82.
- [8] L.F. Dobrzhinetskaya, E.A. Eide, R.B. Larsen, B.A. Sturt, R.G. Trønnes, D.C. Smith, W.R. Taylor, T.V. Posukhova, Microdiamond in high-grade metamorphic rocks of the Western Gneiss Region, Norway, *Geology* 23 (1995) 597–600.
- [9] H.-J. Massonne, A new occurrence of microdiamonds in quartzofeldspathic rocks of the Saxonian Erzgebirge, Germany, and their metamorphic evolution, in: J.J. Gurney, J.L. Gurney, M.D. Pascoe, S.H. Richardson (Eds.), The P.H. Nixon Volume: Proceedings of the VIIth International Kimberlite Conference, Red Roof Design, Cape Town, 1999, pp. 533–539.
- [10] L. Nasdala, H.-J. Massonne, Microdiamonds from the Saxonian Erzgebirge, Germany: in situ micro-Raman characterization, *Eur. J. Mineral.* 12 (2000) 495–498.
- [11] N.D. Chatterjee, R. Krüger, G. Haller, W. Olbricht, The Bayesian approach to an internally consistent thermodynamic database: theory, database, and generation of phase diagrams, *Contrib. Mineral. Petrol.* 133 (1998) 149–168.
- [12] S.-L. Huang, P. Shen, H.-T. Chu, T.-F. Yui, Nanometer-size  $\alpha$ -PbO<sub>2</sub>-type TiO<sub>2</sub> in garnet: A thermobarometer for ultrahigh-pressure metamorphism, *Science* 288 (2000) 321–324.
- [13] J.S. Olsen, L. Gerward, J.Z. Jiang, On the rutile/ $\alpha$ -PbO<sub>2</sub>-type phase boundary of TiO<sub>2</sub>, *J. Phys. Chem. Solids* 60 (1999) 229–233.
- [14] K. Ye, B. Cong, D. Ye, The possible subduction of continental material to depths greater than 200 km, *Nature* 407 (2000) 734–736.
- [15] L. Dobrzhinetskaya, H.W. Green II, S. Wang, Alpe Arami: a peridotite massif from depths more than 300 km, *Science* 271 (1996) 1841–1845.

- [16] K.N. Bozhilov, H.W. Green II, L. Dobrzhinetskaya, Clinoenstatite in Alpe Arami peridotite: additional evidence of very high pressure, *Science* 284 (1999) 128–132.
- [17] H.L.M. vanRoermund, M.R. Drury, Ultra-high pressure ( $P > 6$  GPa) garnet peridotites in western Norway: exhumation of mantle rocks from  $> 185$  km depth, *Terra Nova* 10 (1998) 295–301.
- [18] H.L.M. vanRoermund, M.R. Drury, A. Barnhoorn, A. DeRonde, Non-silicate inclusions in garnet from an ultra-deep orogenic peridotite, *Geol. J.* 35 (2000) 209–229.
- [19] R.Y. Zhang, J.F. Shu, H.K. Mao, J.G. Liou, Magnetite lamellae in olivine and clinohumite from Dabie UHP ultramafic rocks, central China, *Am. Mineral.* 84 (1999) 564–569.
- [20] L.-E. Ricou, J.P. Burg, I. Godfriaux, Z. Ivanov, Rhodope and Vardar: the metamorphic and the olistostromic paired belts related to the Cretaceous subduction under Europe, *Geodin. Acta* 11 (1998) 285–309.
- [21] D.A. Dinter, Late Cenozoic extension of the Alpine collisional orogen, northeastern Greece: Origin of the north Aegean basin, *Geol. Soc. Am. Bull.* 110 (1998) 1208–1230.
- [22] S.R. Barr, S. Temperley, J. Tarney, Lateral growth of the continental crust through deep level subduction-accretion: a re-evaluation of central Greek Rhodope, *Lithos* 46 (1999) 69–94.
- [23] E. Mposkos, A. Krohe, Petrological and structural evolution of continental high pressure (HP) metamorphic rocks in the Alpine Rhodope Domain (N. Greece), in: I. Panayides, C. Xenophontos, J. Malpas (Eds.), Proceedings of the Third International Conference on the Geology of the Eastern Mediterranean, Geological Survey of Cyprus, Nicosia, 2000, pp. 221–232.
- [24] D.K. Kostopoulos, N.M. Ioannidis, S.A. Sklavounos, A new occurrence of ultrahigh-pressure metamorphism, central Macedonia, northern Greece: Evidence from graphitized diamonds?, *Int. Geol. Rev.* 42 (2000) 545–554.
- [25] R.Y. Zhang, J.G. Liou, W.G. Ernst, R.G. Coleman, N.V. Sobolev, V.S. Shatsky, Metamorphic evolution of diamond-bearing and associated rocks from the Kokchetav Massif, northern Kazakhstan, *J. Metamorph. Geol.* 15 (1997) 479–496.
- [26] J.G. Liou, R.Y. Zhang, Occurrences of intergranular coesite in ultrahigh- $P$  rocks from the Sulu region, eastern China: implications for lack of fluid during exhumation, *Am. Mineral.* 81 (1996) 1217–1221.
- [27] A. Wain, D. Waters, A. Jephcoat, H. Olijnyk, The high-pressure to ultrahigh-pressure eclogite transition in the Western Gneiss Region, Norway, *Eur. J. Mineral.* 12 (2000) 667–687.
- [28] J.L. Mosenfelder, S.R. Bohlen, Kinetics of the coesite to quartz transformation, *Earth Planet. Sci. Lett.* 153 (1997) 133–147.
- [29] Y. Ogasawara, M. Ohta, K. Fukasawa, I. Katayama, S. Maruyama, Diamond-bearing and diamond-free metacarbonate rocks from Kumdy-Kol in the Kokchetav Massif, northern Kazakhstan, *Island Arc* 9 (2000) 400–416.
- [30] J.D. Pasteris, B. Wopenka, Raman spectra of graphite as indicators of degree of metamorphism, *Can. Mineral.* 29 (1991) 1–9.
- [31] B. Wopenka, J.D. Pasteris, Structural characterization of kerogens to granulite-facies graphite: applicability of Raman microprobe spectroscopy, *Am. Mineral.* 78 (1993) 533–557.
- [32] M. Yoshikawa, Y. Mori, M. Maegawa, G. Katagiri, H. Ishida, A. Ishitani, Raman scattering from diamond particles, *Appl. Phys. Lett.* 62 (1993) 3114–3116.
- [33] J. Chen, S.Z. Deng, J. Chen, Z.X. Yu, N.S. Xu, Graphitization of nanodiamond powder annealed in argon ambient, *Appl. Phys. Lett.* 74 (1999) 3651–3653.
- [34] Y. Kawasima, G. Katagiri, Fundamentals, overtones, and combinations in the Raman spectrum of graphite, *Phys. Rev. B* 52 (1995) 10053–10059.
- [35] Z. Wang, X. Huang, R. Xue, L. Chen, Dispersion effects of Raman lines in carbons, *J. Appl. Phys.* 84 (1998) 227–231.
- [36] Y.G. Gogotsi, A. Kailer, K.G. Nickel, Pressure-induced phase transformations in diamond, *J. Appl. Phys.* 84 (1998) 1299–1304.
- [37] K.D. Collerson, S. Hapugoda, B.S. Kamber, Q. Williams, Rocks from the mantle transition zone. Majorite-bearing xenoliths from Malaita, southwest Pacific, *Science* 288 (2000) 1215–1223.
- [38] S. Ono, Stability limits of hydrous minerals in sediment and mid-ocean ridge basalt compositions. Implications for water transport in subduction zones, *J. Geophys. Res.* 103 (1998) 18253–18267.
- [39] M. Akaogi, S. Akimoto, Pyroxene–garnet solid-solution equilibria in the systems  $Mg_4Si_4O_{12}$ – $Mg_3Al_2Si_3O_{12}$  and  $Fe_4Si_4O_{12}$ – $Fe_3Al_2Si_3O_{12}$  at high pressures and temperatures, *Phys. Earth Planet. Int.* 15 (1977) 90–106.